

Non-Linear Correlation Functions and Zero-Point Energy Flow in Mixed Quantum-Classical Semiclassical Dynamics

Shreyas Malpathak and Nandini Ananth^{a)}

Department of Chemistry and Chemical Biology, Baker Laboratory, Cornell University Ithaca, 14853 NY, USA

(Dated: 7 November 2022)

Mixed Quantum Classical (MQC)-IVR is a recently introduced semiclassical framework that allows for selective quantization of the modes of a complex system. In the quantum limit, MQC reproduces the semiclassical Double Herman-Kluk IVR results, accurately capturing nuclear quantum coherences and conserving zero-point energy. However, in the classical limit, while MQC mimics the Husimi-IVR for real-time correlation functions with linear operators, it is significantly less accurate for non-linear correlation functions with errors even at time zero. Here, we identify the origin of this discrepancy in the MQC formulation and propose a modification. We analytically show that the modified MQC approach is exact for all correlation functions at time zero, and in a study of zero-point energy (ZPE) flow, we numerically demonstrate that it correctly obtains the quantum and classical limits as a function of time. Interestingly, while classical-limit MQC simulations show the expected, unphysical ZPE leakage, we find it is possible to predict and even modify the direction of ZPE flow through selective quantization of the system, with the quantum-limit modes accepting energy additions but preserving the minimum quantum mechanically required energy.

I. INTRODUCTION

Probing the effects of the quantum nature of nuclei and nuclear-electronic coupling in chemical and biological systems has been the focus of extensive research in recent years.^{1–3} Numerically exact methods to simulate quantum dynamics have found applications in chemical systems of modest sizes^{4,5} but their expensive scaling with system size remains a challenge. Path integral based methods that rely on classical trajectories, such as Matsubara dynamics,^{6,7} Ring Polymer Molecular Dynamics (RPMD),^{8,9} Centroid Molecular Dynamics (CMD),^{10,11} and Multistate Ring Polymer Molecular Dynamics^{12,13} have significantly more favorable scaling laws, but fail to capture nuclear quantum coherences.

Semiclassical (SC) Initial Value Representation (IVR) methods have emerged as a rigorous alternative for the simulation of quantum processes using near-classical trajectories. A hierarchy of SC approximations have been established with the most accurate, quantum-limit SC methods able to describe quantum effects such as zero point energy, tunneling, nonadiabatic and interference effects.^{14,15} Unfortunately, these quantum-limit methods require the evaluation of a complex oscillatory integrand and the resulting numerical sign problem limits applications to high-dimensional systems. Classical-limit SC methods, like Linearized SC-IVR,^{16,17} do not capture interference effects but employ only classical trajectories making them suitable for the simulation of condensed phase processes where quantum coherences are short-lived.^{18–20}

The recently introduced mixed quantum-classical SC method, MQC-IVR,^{21–23} has been shown to reduce the cost of quantum-limit SC correlation function calculations using a modified Filinov filtration technique^{24–26} to mitigate the effects of oscillatory phase. In the limit of small Filinov filter

for all degrees of freedom (dofs) the MQC correlation function becomes identical to a quantum-limit SC-IVR correlation function, specifically the Double Herman-Kluk IVR (DHK-IVR).^{27–30} In the limit of large parameters, for linear operators, MQC corresponds to a classical-limit, linearized method, specifically the Husimi-IVR.^{14,30–34} As the name suggests, the MQC framework uniquely offers a path to selective quantization — by filtering the phase contribution from different dofs to different extents, it is possible to treat some modes in the quantum limit and others in the classical limit.

In previous work, for a range of 1D and 2D model systems, MQC has been numerically shown to gradually tune linear correlation functions from the quantum to the classical limit,^{21,22} and to capture nuclear coherence effects in nonadiabatic scattering models.³⁵ The analytic mixed quantum-classical IVR (AMQC-IVR) method was introduced more recently to treat a handful of system dofs in the quantum-limit while treating the rest in the classical-limit, enabling the calculation of thermal reaction rates in high-dimensional system-bath models.³⁶ Despite these successes, a recent study showed that for correlation functions of operators that are not linear in position and momentum, MQC is less successful particularly in the classical limit where it yields inaccurate values even at time zero.³⁴ Given that both DHK-IVR and Husimi-IVR are, in general, exact for correlation functions at time zero, this is a rather startling observation.

In this paper, we demonstrate the origin of the problem: for operators that are not linear in position and momentum, the classical-limit MQC correlation function does not coincide with the corresponding Husimi-IVR expression. We propose a general strategy to modify MQC such that its classical limit reproduces the Husimi-IVR expression for both linear and non-linear correlation functions. We then use this modified MQC expression to characterize zero-point energy (ZPE) flow in a series of model systems.

Quasi-classical and linearized SC methods typically exhibit ZPE ‘leakage’ in time, with high frequency modes losing zero-point energy to lower frequency ones.^{37–39} This non-

^{a)}Electronic mail: ananth@cornell.edu

conservation of ZPE is attributed to the use of classical trajectories without associated phase terms that are necessary to capture interference effects, and over the years, several mitigation strategies have been proposed.^{37,38,40–52} In contrast, quantum-limit SC methods like DHK-IVR have been shown to conserve ZPE in model systems.⁵³ Here, we investigate ZPE flow in MQC simulations where the strength of Filinov filter is varied from the quantum limit to the classical limit. We then demonstrate strategies to control and indeed direct ZPE flow in the mixed quantum-classical limit using a coupled oscillator model systems constructed to mimic the network of connections observed in realistic systems.

The paper is organized as follows: Sec. II begins with a brief review of the Wigner and Husimi phase space formulations of quantum mechanics, inspects the MQC expression for non-linear correlation functions in the classical limit, and suggests a general strategy to modify MQC. Sec. III describes the model coupled oscillator systems studied here, Sec. IV demonstrates how ZPE flow in these models can be modified by tuning the extent of quantization of the individual oscillators, and Sec. V concludes.

II. THEORY

A. Phase-space formulation of Quantum Mechanics

In the phase space formulation of quantum mechanics,^{54,55} expectation values of operators are calculated analogous to classical mechanics,

$$\langle \hat{B} \rangle = \int d\mathbf{z} \rho(\mathbf{z}) B(\mathbf{z}), \quad (1)$$

where $\mathbf{z} = (p, q)$ is the phase space point, and the functional form of the phase space density $\rho(\mathbf{z})$ and the function $B(\mathbf{z})$ corresponding to \hat{B} vary based on the formulation. Using Cohen's unified classification framework,⁵⁴ the phase space density is expressed as,

$$\rho(\mathbf{z}) = \frac{1}{4\pi^2} \int_{-\infty}^{\infty} d\zeta \int_{-\infty}^{\infty} d\eta f(\xi, \eta) \times \text{Tr} \left[e^{i\zeta(\hat{x}-x) + i\eta(\hat{p}-p)} \hat{\rho} \right], \quad (2)$$

and the phase space function of \hat{B} as,

$$B(\mathbf{z}) = \frac{2\pi\hbar}{4\pi^2} \int_{-\infty}^{\infty} d\zeta \int_{-\infty}^{\infty} d\eta f^{-1}(\xi, \eta) \times \text{Tr} \left[e^{i\zeta(\hat{x}-x) + i\eta(\hat{p}-p)} \hat{B} \right]. \quad (3)$$

The function $f(\xi, \eta)$ in Eq. 3 takes different forms in the Wigner⁵⁶ and Husimi⁵⁷ phase space formulation of quantum mechanics.

In the Wigner formulation,

$$f(\xi, \eta) = 1, \quad (4)$$

resulting in,

$$\rho_W(\mathbf{z}) = \frac{1}{2\pi\hbar} \int d\Delta \left\langle q + \frac{\Delta}{2} \left| \hat{\rho} \right| q - \frac{\Delta}{2} \right\rangle e^{-ip\Delta/\hbar}, \quad (5)$$

and,

$$B_W(\mathbf{z}) = \int d\Delta \left\langle q + \frac{\Delta}{2} \left| \hat{B} \right| q - \frac{\Delta}{2} \right\rangle e^{-ip\Delta/\hbar}. \quad (6)$$

Comparing Eq. 5 and Eq. 6, we see that the Wigner correspondence rules for the density operator and for general operators \hat{B} differ only by a factor of $(2\pi\hbar)^{-1}$ that ensures the phase space density is normalized.

In the Husimi formulation, the correspondence rules are different with,

$$f(\xi, \eta) = e^{-\frac{\xi^2}{4\gamma} - \frac{\hbar^2\gamma}{4}\eta^2}, \quad (7)$$

resulting in,

$$\rho_H(\mathbf{z}) = \frac{1}{2\pi\hbar} \langle \mathbf{z} | \hat{\rho} | \mathbf{z} \rangle, \quad (8)$$

and,

$$\begin{aligned} \tilde{B}_H(\mathbf{z}) &= \frac{2\pi\hbar}{4\pi^2} \int_{-\infty}^{\infty} d\zeta \int_{-\infty}^{\infty} d\eta e^{\frac{\zeta^2}{4\gamma} + \frac{\hbar^2\gamma}{4}\eta^2} \\ &\times \text{Tr} \left[e^{i\zeta(\hat{x}-x) + i\eta(\hat{p}-p)} \hat{\rho} \right] \\ &\neq \langle \mathbf{z} | \hat{B} | \mathbf{z} \rangle, \end{aligned} \quad (9)$$

referred to as the *anti-Husimi* transform of \hat{B} . Here, $|\mathbf{z}\rangle$ is a coherent state with width γ centered at \mathbf{z} ,

$$\langle x | \mathbf{z} \rangle = \left(\frac{\gamma}{\pi} \right)^{1/4} e^{-\frac{\gamma}{2}(x-q)^2 + ip(x-q)/\hbar}. \quad (10)$$

The Husimi density in Eq. 8 is proportional to the diagonal coherent state matrix element of the density operator, whereas this is not true for a general operator \hat{B} , except in special cases like $\hat{B} \equiv \hat{x}$ or \hat{p} . It is this difference that changes the accuracy of the classical-limit of the MQC correlation function even at time zero, as shown in II B.

To find the anti-Husimi transform of an operator, it is useful to establish a connection between the Wigner and Husimi functions,⁵⁸

$$B_H(\mathbf{z}) = \hat{\mathcal{G}}(\gamma; q) \hat{\mathcal{G}}(\gamma^{-1}\hbar^{-2}; p) B_W(\mathbf{z}), \quad (11)$$

$$\tilde{B}_H(\mathbf{z}) = \hat{\mathcal{G}}^{-1}(\gamma; q) \hat{\mathcal{G}}^{-1}(\gamma^{-1}\hbar^{-2}; p) B_W(\mathbf{z}), \quad (12)$$

and,

$$B_H(\mathbf{z}) = \hat{\mathcal{G}}\left(\frac{\gamma}{2}; q\right) \hat{\mathcal{G}}\left(\frac{1}{2}\gamma^{-1}\hbar^{-2}; p\right) \tilde{B}_H(\mathbf{z}), \quad (13)$$

where $\hat{\mathcal{G}}$ is a Gaussian convolution operator defined as,

$$\hat{\mathcal{G}}(\gamma; x) f(x) \equiv \left(\frac{\gamma}{\pi} \right)^{1/2} \int dx' e^{-\gamma(x-x')^2} f(x') \quad (14)$$

$$= e^{\frac{1}{4\gamma} \frac{d^2}{dx^2}} f(x). \quad (15)$$

B. MQC Correlation Functions at Time Zero

A general, real-time quantum correlation function can be expressed as,

$$C_{AB}(t) = \text{Tr} [\hat{\rho} \hat{A} \hat{B}(t)]. \quad (16)$$

where \hat{H} is the system Hamiltonian, $\hat{\rho}$ is the density, and \hat{A} and \hat{B} are the operators evaluated at time zero and time t respectively. Evaluated in a phase space formulation, this expression is,

$$C_{AB}(t) = \int d\mathbf{z} [\hat{\rho} \hat{A}] (\mathbf{z}) [\hat{B}(t)] (\mathbf{z}), \quad (17)$$

where $[\cdot] (\mathbf{z})$ is the phase space function of the operator. In the following sections, for simplicity, we discuss the time dependence of expectation values (corresponding to $\hat{A} = \hat{1}$) noting that all the expressions derived can be applied to correlation functions by replacing $\hat{\rho}$ with $\hat{\rho} \hat{A}$.

The MQC correlation function is obtained by Filinov filtering the phase of the quantum-limit DHK-IVR correlation function to obtain a phase space expression.^{21,22} Here we consider the MQC approximation to the time-dependent expectation value of a general operator \hat{B} for a 1D system

$$\begin{aligned} \langle \hat{B}(t) \rangle_{\text{MQC}} &= \frac{1}{(2\pi)^2} \int d\mathbf{z}_0 \int d\mathbf{z}'_0 D(\mathbf{z}_0, \mathbf{z}'_0, c_p, c_q) \\ &\times \langle \mathbf{z}_0 | \hat{\rho} | \mathbf{z}'_0 \rangle \langle \mathbf{z}'_t | \hat{B} | \mathbf{z}_t \rangle e^{i[S_t(\mathbf{z}_0) - S_t(\mathbf{z}'_0)]} \\ &\times e^{-\frac{1}{2}c_q \Delta_{q0}^2} e^{-\frac{1}{2}c_p \Delta_{p0}^2}, \end{aligned} \quad (18)$$

working in atomic units with $\hbar = 1$ a.u. In Eq. 18, $\hat{\rho}$ is the initial density operator for the system, $D(\mathbf{z}_0, \mathbf{z}'_0, c_p, c_q)$ is the MQC prefactor, c_q and c_p are Filinov parameters, and $\Delta_{x0} = x_0 - x'_0$ for $x \in \{p, q\}$ are the difference variables. The phase space variables, \mathbf{z}_t and \mathbf{z}'_t , in Eq. 18 are obtained by propagating classical trajectories for time t under the classical Hamiltonian with initial conditions, \mathbf{z}_0 , and \mathbf{z}'_0 , respectively, and $S_t(\mathbf{z}_0)$ and $S_t(\mathbf{z}'_0)$ are the actions of forward and backward trajectories respectively.

At time zero, the MQC prefactor is simply

$$D = \sqrt{(c_q + \gamma)(\gamma^{-1} + c_p)}, \quad (19)$$

and the expectation value is,

$$\begin{aligned} \langle \hat{B}(0) \rangle_{\text{MQC}} &= \frac{\sqrt{(c_q + \gamma)(\gamma^{-1} + c_p)}}{(2\pi)^2} \int d\mathbf{z}_0 \int d\mathbf{z}'_0 \langle \mathbf{z}_0 | \hat{\rho} | \mathbf{z}'_0 \rangle \\ &\times \langle \mathbf{z}'_0 | \hat{B} | \mathbf{z}_0 \rangle e^{-\frac{1}{2}c_q \Delta_{q0}^2} e^{-\frac{1}{2}c_p \Delta_{p0}^2}. \end{aligned} \quad (20)$$

For $\mathbf{c} = \{c_p, c_q\} = 0$, Eq. (20) reduces to the DHK expression,

$$\begin{aligned} \langle \hat{B}(0) \rangle_{\text{DHK}} &= \lim_{\mathbf{c} \rightarrow 0} \langle \hat{B}(0) \rangle_{\text{MQC}} \\ &= \frac{1}{(2\pi)^2} \int d\mathbf{z}_0 \int d\mathbf{z}'_0 \langle \mathbf{z}_0 | \hat{\rho} | \mathbf{z}'_0 \rangle \langle \mathbf{z}'_0 | \hat{B} | \mathbf{z}_0 \rangle \\ &= \text{Tr} [\hat{\rho} \hat{B}(0)] = \langle \hat{B}(0) \rangle_{\text{exact}}, \end{aligned} \quad (21)$$

where we use the coherent state completeness relation,

$$\hat{1} = \frac{1}{2\pi} \int d\mathbf{z}_0 |\mathbf{z}_0\rangle \langle \mathbf{z}_0|. \quad (22)$$

In the classical limit (large Filinov parameters), the MQC expectation value is

$$\begin{aligned} \lim_{\mathbf{c} \rightarrow \infty} \langle \hat{B}(0) \rangle_{\text{MQC}} &= \frac{1}{2\pi} \int d\mathbf{z}_0 \langle \mathbf{z}_0 | \hat{\rho} | \mathbf{z}_0 \rangle \langle \mathbf{z}_0 | \hat{B} | \mathbf{z}_0 \rangle \\ &\neq \int d\mathbf{z}_0 \rho_H(\mathbf{z}_0) \tilde{B}_H(\mathbf{z}_0) \\ &= \langle \hat{B}(0) \rangle_{\text{exact}}, \end{aligned} \quad (23)$$

where the inequality follows from the definition of \tilde{B}_H in Eq. (9).

We have shown that while MQC is exact at time zero in the quantum limit ($\mathbf{c} \rightarrow 0$), it is not, in general, exact in the classical limit ($\mathbf{c} \rightarrow \infty$). To understand the behaviour of MQC at time zero for finite non-zero values of the Filinov parameter, we insert the identity,⁵⁹

$$\hat{B} = \frac{1}{2\pi} \int d\mathbf{z} \tilde{B}_H(\mathbf{z}) |\mathbf{z}\rangle \langle \mathbf{z}| \quad (24)$$

into Eq. (20) for both $\hat{\rho}$ and \hat{B} ,

$$\langle \hat{B}(0) \rangle_{\text{MQC}} = \frac{\sqrt{(c_q + \gamma)(\gamma^{-1} + c_p)}}{(2\pi)^4} \int d\mathbf{z}_0 \int d\mathbf{z}'_0 \int d\mathbf{z}' \int d\mathbf{z}'' \langle \mathbf{z}_0 | \mathbf{z}' \rangle \tilde{\rho}_H(\mathbf{z}') \langle \mathbf{z}' | \mathbf{z}'_0 \rangle \langle \mathbf{z}'_0 | \mathbf{z}'' \rangle \tilde{B}_H(\mathbf{z}'') \langle \mathbf{z}'' | \mathbf{z}_0 \rangle e^{-\frac{1}{2}c_q \Delta_{q0}^2} e^{-\frac{1}{2}c_p \Delta_{p0}^2} \quad (25)$$

$$= \int d\mathbf{z} \rho_H(\mathbf{z}) [\mathcal{G}(\tilde{\gamma}_q; q) \mathcal{G}(\tilde{\gamma}_p^{-1}; p) \tilde{B}_H(\mathbf{z})] \quad (26)$$

$$\neq \int d\mathbf{z} \rho_H(\mathbf{z}) \tilde{B}_H(\mathbf{z}) = \langle \hat{B}(0) \rangle_{\text{exact}}, \quad (27)$$

where γ in Eq. (25) is the coherent state width, and $\tilde{\gamma}_q$ and $\tilde{\gamma}_p$ in

Eq. (26) are functions of γ and the Filinov parameters, c_q and

c_p , respectively. Detailed definitions of $\tilde{\gamma}_q$ and $\tilde{\gamma}_p$ are provided in Appendix A along with details of the intermediate steps in the derivation.

The inequality in Eq. (26) indicates that for finite values of the Filinov parameter, MQC is not exact at zero time for a general operator \hat{B} . The exceptions are the position and momentum operators, $\hat{B} \equiv \hat{x}$ or \hat{p} , where

$$\mathcal{G}(\tilde{\gamma}_q; q) \mathcal{G}(\tilde{\gamma}_p^{-1}; p) \tilde{B}_H(\mathbf{z}) = \tilde{B}_H(\mathbf{z}), \quad (28)$$

for all values of \mathbf{c} , a finding that is consistent with previously published numerical results for correlation functions involving these operators.^{21,22}

We have shown that for a general operator, \hat{B} , the MQC correlation function is inaccurate at time zero for non-zero values of the Filinov parameter, and that its classical-limit does not reproduce the Husimi-IVR expression. One potential approach to this problem would be to reformulate MQC by modifying the choice of phase that is filtered. In the next section, we describe a second strategy that allows us to work within the present MQC formalism using a modified operator \hat{B} .

C. Modifying the MQC Correlation Function

Comparing Eq. (26) and Eq. (27) suggests that we can correct the MQC correlation function by replacing operator \hat{B} by a new operator $\hat{\mathcal{B}}$, such that

$$\mathcal{G}(\tilde{\gamma}_q; q) \mathcal{G}(\tilde{\gamma}_p^{-1}; p) \tilde{\mathcal{B}}_H(\mathbf{z}) = \tilde{B}_H(\mathbf{z}). \quad (29)$$

or equivalently using the relationship between the Anti-Husimi transform and the Wigner transform in Eq. (12),

$$\mathcal{G}(\tilde{\gamma}_q; q) \mathcal{G}(\tilde{\gamma}_p^{-1}; p) \mathcal{B}_W(\mathbf{z}) = B_W(\mathbf{z}). \quad (30)$$

The MQC expression with the modified operator is still exact in the quantum limit; when $\mathbf{c} \rightarrow 0$, the Gaussian convolutions in Eq. (29) reduce to delta functions, such that

$$\hat{\mathcal{B}} = \hat{B}. \quad (31)$$

In the classical limit, $\mathbf{c} \rightarrow \infty$, the Filinov-dependent width parameters $\tilde{\gamma}_q \rightarrow \frac{\gamma}{2}$ and $\tilde{\gamma}_p \rightarrow 2\gamma$, and using Eq. (13) we obtain

$$\lim_{\mathbf{c} \rightarrow \infty} \tilde{\mathcal{B}}_H(\mathbf{z}) = \tilde{B}_H(\mathbf{z}). \quad (32)$$

The modified MQC expression thus achieves the correct form in both the quantum and classical limits, with

$$\lim_{\mathbf{c} \rightarrow 0} \langle \hat{\mathcal{B}}(t) \rangle_{\text{MQC}} = \langle \hat{B}(t) \rangle_{\text{DHK}}, \quad (33)$$

and

$$\lim_{\mathbf{c} \rightarrow \infty} \langle \hat{\mathcal{B}}(t) \rangle_{\text{MQC}} = \langle \hat{B}(t) \rangle_{\text{Hus}}. \quad (34)$$

Although our analysis and derivation of the modified operator is shown here for the expectation value, this idea can be

TABLE I. Parameters for the three model systems (in atomic units).

Model	F	ω_1	ω_2	ω_3	C_{12}	C_{23}	C_{13}
A	2	1.0	0.5	-	10^{-4}	-	-
B	3	1.0	0.5	0.25	10^{-4}	2×10^{-4}	0.0
C	3	1.0	1.0	0.5	10^{-4}	2×10^{-4}	0.0

simply extended to real-time correlation functions resulting in the modified MQC expression,

$$\begin{aligned} C_{AB}(t) &= \frac{1}{(2\pi)^2} \int d\mathbf{z}_0 \int d\mathbf{z}'_0 D(\mathbf{z}_0, \mathbf{z}'_0, c_p, c_q) \\ &\times \langle \mathbf{z}_0 | \hat{\rho} \hat{A} | \mathbf{z}'_0 \rangle \langle \mathbf{z}'_0 | \hat{\mathcal{B}} | \mathbf{z}_t \rangle e^{i[S_t(\mathbf{z}_0) - S_t(\mathbf{z}'_0)]} \\ &\times e^{-\frac{1}{2}c_q \Delta_{q0}^2} e^{-\frac{1}{2}c_p \Delta_{p0}^2}. \end{aligned} \quad (35)$$

Finding the modified operator $\hat{\mathcal{B}}$ can be non-trivial, but for simple operators it is possible to derive an analytic expression. For instance, the modified MQC correlation function when $\hat{B} = \hat{x}^2$ is obtained with the modified operator $\hat{\mathcal{X}}^2$,

$$\hat{x}^2 \rightarrow \hat{\mathcal{X}}^2 = \hat{x}^2 - \frac{c_p}{1 + \gamma c_p}, \quad (36)$$

and similarly the modified MQC correlation function for $\hat{B} = \hat{p}^2$ is obtained with the modified operator, $\hat{\mathcal{P}}^2$,

$$\hat{p}^2 \rightarrow \hat{\mathcal{P}}^2 = \hat{p}^2 - \frac{\gamma c_q}{\gamma + c_q}. \quad (37)$$

III. MODEL SYSTEM AND SIMULATION DETAILS

Inspired by a model previously used to study ZPE leakage in SC dynamics,⁵³ we consider three different models of coupled harmonic oscillators with cubic couplings,

$$V(x_1, \dots, x_F) = \sum_{i=1}^F \frac{1}{2} m \omega_i^2 x_i^2 + \sum_{i < j} C_{ij} (x_i - x_j)^3, \quad (38)$$

where F is number of degrees of freedom, all oscillators have mass $m = 1$ a.u., ω_i is the frequency of the i^{th} oscillator, and C_{ij} is the pair-wise coupling between oscillators. Model A is a two dimensional model — two harmonic oscillators with cubic coupling. Models B and C are three dimensional models where one oscillator is weakly coupled to a subsystem comprising two strongly coupled oscillators. In model C, two weakly coupled oscillators have the same frequency to explore the effect of having resonant modes treated with different levels of quantization. Frequencies of the oscillators and coupling constants for all models are listed in Table I.

We chose the initial coherent state $|\psi_i\rangle \equiv |\mathbf{z}_i\rangle$ to correspond to the ground-state of the uncoupled harmonic oscillators, a product of coherent states with widths $\gamma_i = m\omega_i$, centered at $\mathbf{z}_i = (0, 0)$. Since the magnitude of the coupling constants is very small, the overlap between the initial state and the ground state of the coupled system is nearly unity ensuring that only

the lowest vibrational state for each oscillator is populated. The total energy can then be written as,

$$E = \sum_i E_i \quad (39)$$

where the E_i is the ZPE of the i^{th} oscillator.⁵³

To track the flow of ZPE, we calculate the energy expectation value of each oscillator as a function of time,

$$\langle \hat{E}_i(t) \rangle = \frac{1}{2m} \langle \hat{p}_i^2(t) \rangle + \frac{1}{2} m \omega_i^2 \langle \hat{x}_i^2(t) \rangle. \quad (40)$$

In our modified MQC implementation, the energy expectation value in Eq. 40 is calculated by evaluating two independent non-linear correlation functions using Eq. (35). Specifically, the $\langle \hat{x}_i^2(t) \rangle$ term is obtained using modified operator $\hat{\mathcal{B}} = \hat{\chi}_i^2(t)$ defined in Eq. (36) and the $\langle \hat{p}_i^2(t) \rangle$ term is obtained using modified operator $\hat{\mathcal{B}} = \hat{\pi}_i^2(t)$ defined in Eq. (37). Numerical integrals are evaluated using standard Monte Carlo techniques with the sampling function,

$$\rho(\mathbf{z}_0, \mathbf{z}'_0) = \mathcal{N} |\langle \mathbf{z}_0 | \psi_i \rangle \langle \psi_i | \mathbf{z}'_0 \rangle| e^{-\frac{1}{2}(\mathbf{q}_0 - \mathbf{q}'_0)^T \cdot \mathbf{c}_q \cdot (\mathbf{q}_0 - \mathbf{q}'_0)} \times e^{-\frac{1}{2}(\mathbf{p}_0 - \mathbf{p}'_0)^T \cdot \mathbf{c}_p \cdot (\mathbf{p}_0 - \mathbf{p}'_0)}, \quad (41)$$

where \mathcal{N} ensures proper normalization. Note that while the sampling is performed using sum and difference variables, we then transform back into the $(\mathbf{z}_0, \mathbf{z}'_0)$ for trajectory propagation and calculation of the estimator. Trajectories are propagated under the classical Hamiltonian using a fourth-order symplectic integrator⁶⁰ with a timestep of 0.1 a.u. for Model A, and 0.175 a.u. for models B and C to ensure total energy conservation. All calculations presented here were converged to within the error bars shown using at most 10^7 trajectories.

Finally, we note that we renormalize the energy in each mode such that the total energy stays constant at all times, $\sum_{i=1}^F \langle \hat{E}_i(t) \rangle = \sum_{i=1}^F \langle \hat{E}_i(0) \rangle$. This is required because SC methods used here are, at best, only approximately unitary.^{61–65}

IV. RESULTS AND DISCUSSION

Using similar model systems, previous work has established that DHK-IVR, a quantum-limit SC method, conserves ZPE whereas LSC-IVR, a classical-limit SC method does not.⁵³ Here, we use the modified MQC method to establish the extent of ZPE leakage in dynamics that employ finite values of the Filinov parameter. Further, we investigate how selective quantization of modes influences ZPE flow, with the potential to limit the extent to which the unphysical flow of energy occurs within a subsystem.

In Fig. 1, we demonstrate that the modified MQC expression, unlike the original, reproduces the exact values for the energy expectation value of a single oscillator in 2D model A for all values of the Filinov parameter. We also show that the classical limit of the modified MQC also correctly reproduces the Husimi IVR result with significant ZPE leakage.

Having established the accuracy of the modified MQC expression in capturing both quantum-limit and classical-limit

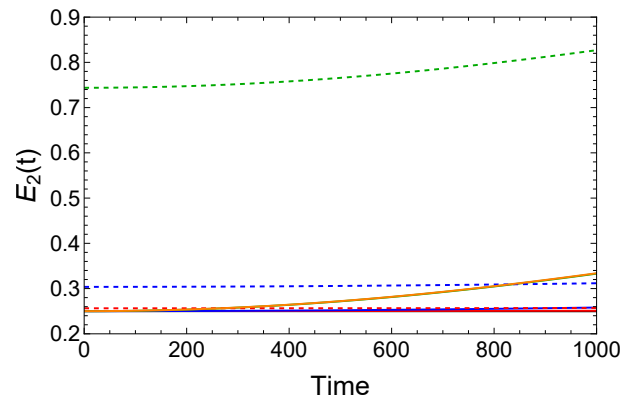


FIG. 1. We plot the energy expectation value for the low frequency oscillator 2 as a function of time for model A. The original MQC results are shown using dashed lines and compared against the modified MQC method shown using solid lines for different values of the Filinov parameter $c = 0.01$ (red), $c = 0.1$ (blue), and $c = 100$ (green). Results from DHK-IVR (black) and Husimi-IVR (orange) are also shown for reference. Note that in the quantum-limit, $c = 0.01$ both the original and modified MQC results coincide with the DHK-IVR result, whereas in the classical limit, $c = 100$, only the modified MQC reproduces the Husimi-IVR results with the original formulation yielding results that are significantly different even at time zero.

SC dynamics, we explore the extent to which this method conserves ZPE for different values of the Filinov parameter. In Fig. 2 we plot the average energies of the two oscillators in model A. As expected, DHK-IVR and quantum-limit MQC, $\mathbf{c}_1 = \mathbf{c}_2 = \mathbf{c} = 0.01$, both show ZPE conservation for the length of the simulation. On the other hand, Husimi-IVR and classical-limit MQC, ($\mathbf{c} = 100$), both exhibit significant loss of ZPE with unphysical energy flow from the high frequency oscillator into the low frequency one. As the Filinov parameter is increased, we see a systematic onset of ZPE leakage from the high frequency mode, consistent with the idea that SC methods rely on interference to conserve ZPE. It is notable that despite increasing the Filinov parameter 10-fold, MQC with $c = 0.1$ still exhibits reasonable ZPE conservation and requires far few trajectories for convergence than the corresponding $c = 0.01$ MQC simulation.

Working with 2D model A, we also perform MQC simulations where one mode is treated in the quantum limit while the other is described in the classical limit. In Fig. 3, we demonstrate that the mode that is treated in the quantum limit does indeed conserve ZPE, whereas the classical-limit mode does not. Interestingly, when we quantize the low frequency oscillator, there is no observed change in ZPE flow with the classical-limit high-frequency mode continuing to lose energy. However, when we treat the high frequency mode in the quantum limit, we stem the loss of energy from this mode and instead see a reversal with energy flowing uphill from the classical-limit low-frequency mode.

Model B offers a more interesting test case for mixed quantization. For this model, in the quantum limit, all three oscillators conserve ZPE as shown in Fig. 4, and in the classical limit, we see rapid ZPE exchange between the two lower fre-

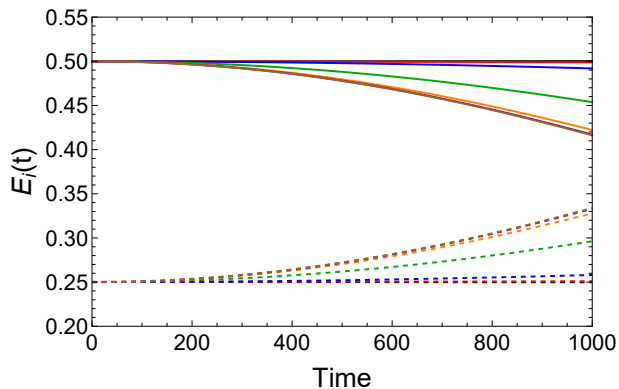


FIG. 2. We plot the energies of high frequency oscillator 1 (solid lines) and low frequency oscillator 2 (dashed lines) as a function of time for Model A calculated using DHK-IVR (black), MQC with $c = 0.01$ (red), $c = 0.1$ (blue), $c = 1$ (green), $c = 10$ (orange), $c = 100$ (purple), and Husimi-IVR (brown). DHK-IVR results overlap with $c = 0.01$, and Husimi-IVR results overlap with $c = 100$. As expected, the extent of ZPE leakage increases systematically as the value of Filinov parameters is increased

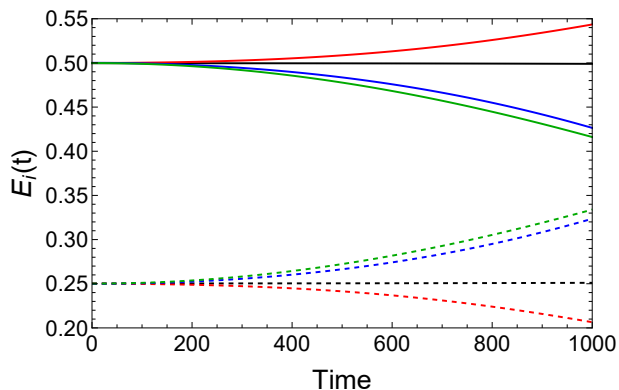


FIG. 3. We plot the individual oscillator energies obtained when performing a mixed quantum-classical MQC simulation with the energy of the high frequency mode (oscillator 1) shown using solid lines and the low frequency mode (oscillator 2) shown with dashed lines. Results obtained by treating all modes in the quantum limit with $c_1 = c_2 = 0.01$ are shown in black and compared against two mixed-limit cases with $c_1 = 0.01, c_2 = 100$ (red), and $c_1 = 100, c_2 = 0.01$ (blue), as well as the classical limit $c_1 = c_2 = 100$ (green).

quency oscillators that are strongly coupled, with the weakly coupled high frequency oscillator losing ZPE to the other two modes on a longer timescale. In the first study of mixed quantization, we treat the high frequency oscillator in the quantum limit while describing the rest in the classical limit. As shown in Fig. 4(a), we find that the classical ‘bath’ oscillators continue to exchange ZPE but the quantum-limit oscillator approximately conserves ZPE over a significantly longer timescale (by a factor of 2) with some increase in energy corresponding to leakage from the classical subsystem.

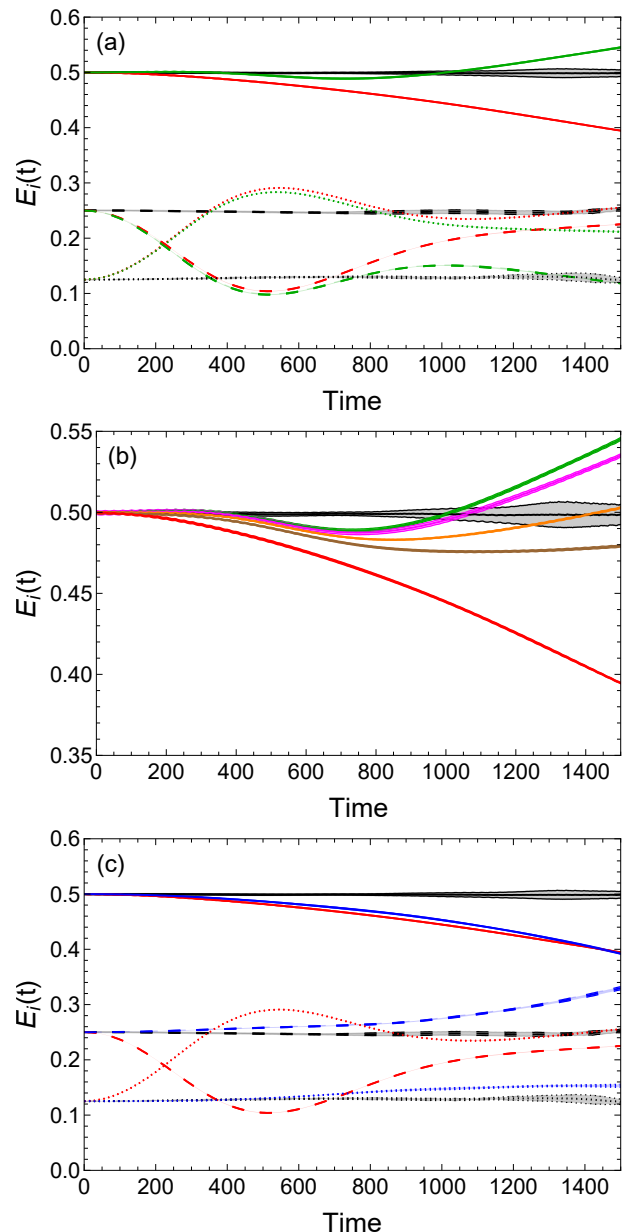


FIG. 4. We plot the energy as a function of time in oscillators 1 (solid), 2 (dashed) and 3 (dotted) in model B. MQC results in the quantum-limit ($c = 0.01$, black) and classical-limit ($c = 1000$, red) are shown in all panels and compared with different versions of mixed quantization. (a) weakly coupled high frequency oscillator 1 is treated in the quantum limit, while the other two strongly coupled lower frequency modes are treated classically, $c_1 = 10^{-2}, c_2 = c_3 = 10^3$ (green). (b) Oscillators 2 and 3 are treated classically ($c_2 = c_3 = 10^3$) again, and the Filinov parameter for oscillator 1 is varied — $c_1 = 10^{-2}$ (green), $c_1 = 0.1$ (pink), $c_1 = 0.5$ (orange), and $c_1 = 1$ (brown). (c) The two lower frequency oscillators are treated in the quantum-limit eliminating the fast ZPE exchange observed in the classical-limit simulations with $c_1 = 10^3, c_2 = c_3 = 10^{-2}$ (blue). In all cases, the quantized sub-system conserves ZPE for a significantly longer time compared to the classical-limit, before eventually accepting energy from the classical sub-system. Highlights around lines indicate error bars.

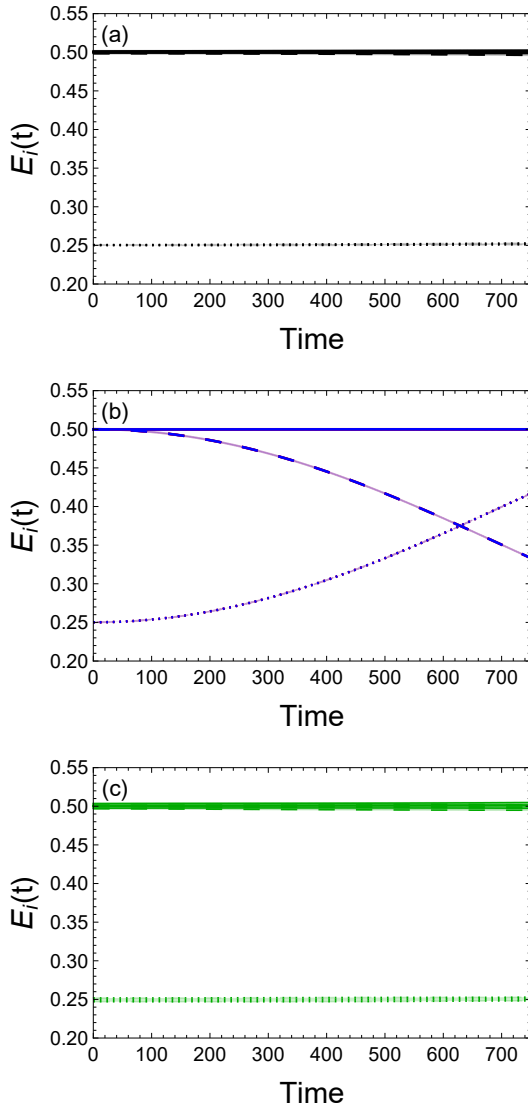


FIG. 5. We plot the energy as a function of time for high frequency oscillators 1 (solid) and 2 (dashed), and low frequency oscillator 3 (dotted) in model C, compared for various different MQC limits —(a) All modes treated in the quantum limit with $\mathbf{c} = 0.01$ (black); (b) All modes treated in the classical limit with $\mathbf{c} = 100$ (red) yield results that are identical to the mixed quantization case where just the weakly coupled oscillator 1 is treated in the quantum limit, $\mathbf{c}_1 = 0.01, \mathbf{c}_2 = \mathbf{c}_3 = 100$ (blue), and (c) We quantize the strongly coupled subsystem of oscillator 2 and 3 with the resonant, high frequency oscillator 1 treated in the classical limit, $\mathbf{c}_1 = 100, \mathbf{c}_2 = \mathbf{c}_3 = 0.01$ (green). Note that in (a) and (c), solid and dashed lines overlap. In (b), results for the two different Filinov parameter values (red and blue) overlap. Highlights around lines indicate error bars.

In a final study of model B, we quantize the strongly coupled subsystem of low frequency oscillators and treat the high frequency oscillator in the classical limit, and plot the results in Fig. 4(c) We find that the quantized subsystem now conserves ZPE with no exchange of energy between the two low

frequency oscillators. There is a net increase in the individual oscillator energies of the subsystem, however, due to energy flowing into the quantized subsystem from the classical-limit, high frequency oscillator.

Model C is similar to model B, but explores how the presence of oscillators of equal frequency (resonant) in the classical and quantum-limit subsystems affects overall ZPE flow. Specifically, we have two weakly coupled high frequency oscillators, one of which is strongly coupled to the low frequency oscillator. If all three are treated in the quantum limit, the expected ZPE conservation is seen in the MQC results in Fig. 5. Interestingly, when all modes are treated in the classical limit, we see some exchange of ZPE between the two strongly coupled oscillators, but no ZPE leakage from the weakly coupled oscillator perhaps as a consequence of the resonance in the model. Given this, quantizing just the weakly coupled oscillator continues to conserve its energy while the classical limit oscillators exhibit ZPE exchange. However, quantizing the strongly coupled oscillators, results in conservation of ZPE - a promising insight into conservation strategies for systems where the quantized subsystem and classical bath share a resonant frequency.

V. CONCLUSIONS

In this paper, we begin with a detailed study of the origin of the MQC SC method's inaccuracy at time zero for non-linear correlation functions. We show that MQC with finite, non-zero values of the Filinov parameter is not exact at time zero for a general operator \hat{B} . Further, we show that the real-time MQC correlation functions in the classical limit does not to the Husimi IVR correlation function. We perform a detailed analysis of the Husimi and Wigner phase space formulation of quantum mechanics and identify a simple modification to correct for both these problems. Specifically, we propose that replacing operator \hat{B} with a new operator that is obtained through inverse Gaussian convolutions of Wigner/Anti-Husimi functions of the original operator. We analytically derive the modified operator for \hat{x}^2 and \hat{p}^2 , and use the resulting expression to characterize ZPE flow in MQC simulations.

We construct a series of model systems comprising oscillators of different frequencies and with different coupling motifs chosen to mimic real system connectivities. We demonstrate that by selective quantization of weakly coupled modes, it is possible to improve the timescale on which ZPE is conserved for a subset of modes. This work establishes a promising path forward to real system simulations using the modified MQC approach proposed here. Next steps include establishing a path to deriving modified operators corresponding to other operators, including most notably the projection operator.

ACKNOWLEDGMENTS

This work was funded, in part, by NSF CAREER Grant No. CHE 1555205. The authors thank Jennifer Mavroudakis for helpful discussions.

Appendix A: Detailed derivation of the modified MQC method

Starting with Eq.(25), we note that the integrals over \mathbf{z}_0 and \mathbf{z}'_0 can be evaluated analytically to yield,

$$\begin{aligned} \langle \hat{B}(0) \rangle_{\text{MQC}} &= \frac{\sqrt{(c_q + \gamma)(\gamma^{-1} + c_p)}}{(2\pi)^4} \int d\mathbf{z}_0 \int d\mathbf{z}'_0 \int d\mathbf{z}' \int d\mathbf{z}'' \langle \mathbf{z}_0 | \mathbf{z}' \rangle \tilde{\rho}_H(\mathbf{z}') \langle \mathbf{z}' | \mathbf{z}'_0 \rangle \langle \mathbf{z}'_0 | \mathbf{z}'' \rangle \tilde{B}_H(\mathbf{z}'') \langle \mathbf{z}'' | \mathbf{z}_0 \rangle e^{-\frac{1}{2}c_q \Delta_{q_0}^2} e^{-\frac{1}{2}c_p \Delta_{p_0}^2} \\ &= \frac{1}{2\pi} \sqrt{\frac{\gamma_q}{\pi}} \sqrt{\frac{1}{\gamma_p \pi}} \int d\mathbf{z}' \int d\mathbf{z}'' e^{-\gamma_q (q' - q'')^2} e^{-\gamma_p^{-1} (p' - p'')^2} \tilde{\rho}_H(\mathbf{z}') \tilde{B}_H(\mathbf{z}'') \end{aligned} \quad (\text{A1})$$

where $\gamma_q = \frac{\gamma}{2} \frac{\gamma^{-1} + c_p}{\gamma^{-1} + 2c_p}$, and $\gamma_p^{-1} = \frac{1}{2\gamma} \frac{c_q + \gamma}{2c_q + \gamma}$. We then split the Gaussian convolution with width γ_3 into two separate Gaussian convolutions with widths γ_1 and γ_2 ,

$$\sqrt{\frac{\gamma_3}{\pi}} \int dx' e^{-\gamma_3 (x - x')^2} f(x') = \sqrt{\frac{\gamma_1}{\pi}} \int dx'' e^{-\gamma_1 (x - x'')^2} \left[\sqrt{\frac{\gamma_2}{\pi}} \int dx' e^{-\gamma_2 (x'' - x')^2} f(x') \right], \quad (\text{A2})$$

such that $\gamma_3^{-1} = \gamma_1^{-1} + \gamma_2^{-1}$. We now define $\tilde{\gamma}_q = \frac{\gamma}{2} \frac{\gamma^{-1} + c_p}{c_p}$, and $\tilde{\gamma}_p^{-1} = \frac{1}{2\gamma} \frac{c_q + \gamma}{c_q}$, such that

$$\gamma_q^{-1} = \tilde{\gamma}_q^{-1} + 2\gamma^{-1}, \quad (\text{A3})$$

and

$$\gamma_p = \tilde{\gamma}_p + 2\gamma, \quad (\text{A4})$$

to split the Gaussian convolutions in Eq.(A1) into two Gaussian convolutions each,

$$\langle \hat{B}(0) \rangle_{\text{MQC}} = \frac{1}{2\pi} \int d\mathbf{z} \left[\frac{1}{2\pi} \int d\mathbf{z}' e^{-\frac{\gamma}{2} (q - q')^2} e^{-\frac{1}{2\gamma} (p - p')^2} \tilde{\rho}_H(\mathbf{z}') \right] \left[\sqrt{\frac{\tilde{\gamma}_q}{\pi}} \sqrt{\frac{1}{\tilde{\gamma}_p \pi}} \int d\mathbf{z}'' e^{-\tilde{\gamma}_q (q - q'')^2} e^{-\tilde{\gamma}_p^{-1} (p - p'')^2} \tilde{B}_H(\mathbf{z}'') \right] \quad (\text{A5})$$

$$= \frac{1}{2\pi} \int d\mathbf{z} \left[\mathcal{G} \left(\frac{\gamma}{2}; q \right) \mathcal{G} \left(\frac{1}{2\gamma}; p \right) \tilde{\rho}_H(\mathbf{z}) \right] \times \left[\mathcal{G}(\tilde{\gamma}_q; q) \mathcal{G}(\tilde{\gamma}_p^{-1}; p) \tilde{B}_H(\mathbf{z}) \right] \quad (\text{A6})$$

$$= \int d\mathbf{z} \rho_H(\mathbf{z}) \left[\mathcal{G}(\tilde{\gamma}_q; q) \mathcal{G}(\tilde{\gamma}_p^{-1}; p) \tilde{B}_H(\mathbf{z}) \right]. \quad (\text{A7})$$

To go from Eq.(A5) to Eq.(A6), we have used the definition of a Gaussian convolution from Eq.(14), and then used the relationship between the Husimi transform and the anti-Husimi transform of an operator, Eq.(13), to yield Eq.(A7), which is the same as Eq.(26).

¹J. Cao, R. J. Cogdell, D. F. Coker, H. G. Duan, J. Hauer, U. Kleinekathöfer, T. L. Jansen, T. Mančal, R. J. D. Miller, J. P. Ogilvie, V. I. Prokhorenko, T. Renger, H. S. Tan, R. Tempelaar, M. Thorwart, E. Thyryhaug, S. Westenhoff, and D. Zigmantas, *Science Advances* **6**, (2020).
²T. E. Markland and M. Ceriotti, *Nature Reviews Chemistry* **2**, 1 (2018).
³N. Ananth, *Annual Review of Physical Chemistry* **73**, 299 (2022).
⁴J. Schulze, M. F. Shibl, M. J. Al-Marri, and O. Kühn, *The Journal of Chemical Physics* **144**, 185101 (2016).
⁵N. Lyu, M. B. Soley, and V. S. Batista, *Journal of Chemical Theory and Computation* **18**, 3327 (2022).
⁶T. J. H. Hele, M. J. Willatt, A. Muolo, and S. C. Althorpe, *The Journal of Chemical Physics* **142**, 134103 (2015).
⁷T. J. H. Hele, M. J. Willatt, A. Muolo, and S. C. Althorpe, *The Journal of Chemical Physics* **142**, 191101 (2015).
⁸I. R. Craig and D. E. Manolopoulos, *Journal of Chemical Physics* **121**, 3368 (2004).
⁹I. R. Craig and D. E. Manolopoulos, *The Journal of Chemical Physics* **122**, 084106 (2005).
¹⁰J. Cao and G. A. Voth, *Journal of* **100**, 5106 (1994).
¹¹S. Jang and G. A. Voth, *The Journal of Chemical Physics* **111**, 2371 (1999).
¹²N. Ananth, *The Journal of Chemical physics* **139**, 124102 (2013).
¹³J. R. Duke and N. Ananth, *Faraday Discussions* **195**, 253 (2016).

¹⁴W. H. Miller, *Journal of Physical Chemistry A* **105**, 2942 (2001).
¹⁵W. H. Miller, *The Journal of Physical Chemistry A* **113**, 1405 (2009).
¹⁶H. Wang, X. Sun, and W. H. Miller, *Journal of Chemical Physics* **108**, 9726 (1998).
¹⁷Q. Shi and E. Geva, *The Journal of Chemical Physics* **118**, 8173 (2003).
¹⁸J. Liu, *International Journal of Quantum Chemistry* **115**, 657 (2015).
¹⁹J. A. Poulsen, G. Nyman, and P. J. Rossky, *Proceedings of the National Academy of Sciences* **102**, 6709 (2005).
²⁰X. Sun, P. Zhang, Y. Lai, K. L. Williams, M. S. Cheung, B. D. Dunietz, and E. Geva, *Journal of Physical Chemistry C* **122**, 11288 (2018).
²¹S. V. Antipov, Z. Ye, and N. Ananth, *The Journal of Chemical Physics* **142**, 184102 (2015).
²²M. S. Church, S. V. Antipov, and N. Ananth, *The Journal of Chemical Physics* **146**, 234104 (2017).
²³S. Malpathak, M. S. Church, and N. Ananth, *The Journal of Physical Chemistry A* **126**, 6359 (2022).
²⁴V. Filinov, *Nuclear Physics B* **271**, 717 (1986).
²⁵N. Makri and W. H. Miller, *Chemical Physics Letters* **139**, 10 (1987).
²⁶N. Makri and W. H. Miller, *The Journal of Chemical Physics* **89**, 2170 (1988).
²⁷M. F. Herman and E. Kluk, *Chemical Physics* **91**, 27 (1984).
²⁸K. G. Kay, *The Journal of Chemical Physics* **100**, 4377 (1994).

- ²⁹M. F. Herman, *Chemical Physics Letters* **275**, 445 (1997).
- ³⁰M. Thoss, H. Wang, and W. H. Miller, *The Journal of Chemical Physics* **114**, 9220 (2001).
- ³¹M. F. Herman and D. F. Coker, *The Journal of Chemical Physics* **111**, 1801 (1999).
- ³²Y. Zhao and N. Makri, *Chemical Physics* **280**, 135 (2002).
- ³³N. J. Wright and N. Makri, *The Journal of Physical Chemistry B* **108**, 6816 (2004).
- ³⁴S. L. Choudhury and F. Großmann, *Condensed Matter* **5**, 3 (2020).
- ³⁵M. S. Church, T. J. H. Hele, G. S. Ezra, and N. Ananth, *The Journal of Chemical Physics* **148**, 102326 (2018).
- ³⁶M. S. Church and N. Ananth, *The Journal of Chemical Physics* **151**, 134109 (2019).
- ³⁷J. M. Bowman, B. Gazdy, and Q. Sun, *The Journal of Chemical Physics* **91**, 2859 (1989).
- ³⁸W. H. Miller, W. L. Hase, and C. L. Darling, *The Journal of Chemical Physics* **91**, 2863 (1989).
- ³⁹S. Habershon and D. E. Manolopoulos, *The Journal of Chemical Physics* **131**, 244518 (2009).
- ⁴⁰D. Lu and W. L. Hase, *The Journal of Chemical Physics* **89**, 6723 (1988).
- ⁴¹G. Nyman and J. Davidsson, *The Journal of Chemical Physics* **92**, 2415 (1990).
- ⁴²A. J. C. Varandas and J. M. C. Marques, *The Journal of Chemical Physics* **97**, 4050 (1992).
- ⁴³T. D. Sewell, D. L. Thompson, J. Gezelter, and W. H. Miller, *Chemical Physics Letters* **193**, 512 (1992).
- ⁴⁴R. Alimi, A. García-Vela, and R. B. Gerber, *The Journal of Chemical Physics* **96**, 2034 (1992).
- ⁴⁵G. H. Peslherbe and W. L. Hase, *The Journal of Chemical Physics* **100**, 1179 (1994).
- ⁴⁶K. F. Lim and D. A. McCormack, *The Journal of Chemical Physics* **102**, 1705 (1995).
- ⁴⁷C. Schlier, *The Journal of Chemical Physics* **103**, 1989 (1995).
- ⁴⁸D. A. McCormack and K. F. Lim, *The Journal of Chemical Physics* **103**, 1991 (1995).
- ⁴⁹Y. Guo, D. L. Thompson, and T. D. Sewell, *The Journal of Chemical Physics* **104**, 576 (1996).
- ⁵⁰G. Stock and U. Müller, *The Journal of Chemical Physics* **111**, 65 (1999).
- ⁵¹Z. Xie and J. M. Bowman, *The Journal of Physical Chemistry A* **110**, 5446 (2006).
- ⁵²F. Briec, Y. Bronstein, H. Dammak, P. Depondt, F. Finocchi, and M. Hayoun, *Journal of Chemical Theory and Computation* **12**, 5688 (2016).
- ⁵³M. Buchholz, E. Fallacara, F. Gottwald, M. Ceotto, F. Grossmann, and S. D. Ivanov, *Chemical Physics* **515**, 231 (2018).
- ⁵⁴L. Cohen, *Journal of Mathematical Physics* **7**, 781 (1966).
- ⁵⁵H.-W. Lee, *Physics Reports* **259**, 147 (1995).
- ⁵⁶E. Wigner, *Physical Review* **40**, 749 (1932).
- ⁵⁷K. Husimi, *Proceedings of the Physico-Mathematical Society of Japan* **22**, 264 (1940).
- ⁵⁸J. E. Harriman and M. E. Casida, *International Journal of Quantum Chemistry* **45**, 263 (1993).
- ⁵⁹E. Pollak, S. Upadhyayula, and J. Liu, *The Journal of Chemical Physics* **156**, 244101 (2022).
- ⁶⁰M. L. Brewer, J. S. Hulme, and D. E. Manolopoulos, *The Journal of Chemical Physics* **106**, 4832 (1997).
- ⁶¹M. F. Herman, *The Journal of Chemical Physics* **85**, 2069 (1986).
- ⁶²S. Garashchuk, F. Grossmann, and D. Tannor, *Journal of the Chemical Society, Faraday Transactions* **93**, 781 (1997).
- ⁶³C. Harabati, J. M. Rost, and F. Grossmann, *The Journal of Chemical Physics* **120**, 26 (2004).
- ⁶⁴S. Zhang and E. Pollak, *Journal of Chemical Theory and Computation* **1**, 345 (2005).
- ⁶⁵J. Tatchen, E. Pollak, G. Tao, and W. H. Miller, *The Journal of Chemical Physics* **134**, 134104 (2011).